

HOW WELL DO REDUCED MODELS CAPTURE THE DYNAMICS IN MODELS OF INTERACTING NEURONS ?

YAO LI, LOGAN CHARIKER, AND LAI-SANG YOUNG

Abstract. This paper introduces a class of stochastic models of interacting neurons with emergent dynamics similar to those seen in local cortical populations, and compares them to very simple reduced models driven by the same mean excitatory and inhibitory currents. Discrepancies in firing rates between network and reduced models were investigated, and mechanisms leading to these discrepancies were identified. Chief among them is correlations in spiking, or partial synchronization, working in concert with “nonlinearities” in the time evolution of membrane potentials. Additionally, simple random walk models and their first passage times were shown to reproduce well fluctuations in neuronal membrane potentials and interspike times.

INTRODUCTION

Models in neuroscience come in an extraordinarily wide range, from very simple, seeking to describe complex neural behavior using a few coarse-grained variables, to extremely complex, as in Connectome type projects that seek to provide a complete map of all neuronal connections – with a myriad of possibilities in between. The modeling of individual neurons alone can vary from a single number that describes its firing rate, to an integrate-and-fire equation, or a Hodgkin-Huxley model, or one that treats individual ionic channels and the biochemical reactions that are triggered with each synapse. Needless to say, models that incorporate more neuroanatomical and neurophysiological details are more realistic, but realistic modeling is not without cost: with greater complexity comes more unknown parameters corresponding to quantities that cannot be measured in the laboratory.

A question that we believe has not received adequate attention is: how do models of different levels of complexity compare? One does not expect a reduced model to provide the same kind of detailed information as a large-scale network of spiking neurons, but does it provide useful information, rough but in the ballpark? If not, what causes the discrepancies? What are the mechanisms reduced models lack that cause them to produce inaccurate results?

Clearly, these questions cannot be asked in the abstract; the answer will depend not only on the models but on the type of questions. Until the theory is more advanced, one will have to severely limit one’s scope. In this paper, we report on findings from a study that compares some specific kinds of models of local neuronal populations. Our “detailed” models are stochastic models of interacting neurons

LC was supported by a grant from the Swartz Foundation.
LSY was supported in part by NSF Grant DMS-1363161.

with integrate-and-fire type dynamics; they can be thought of as modeling the dynamical interactions that take place in local circuitries in the mammalian cortex; and our reduced models are either described by simple ODEs of Wilson-Cowan type or by random walks in the space of membrane potentials.

It soon became clear that even after specifying what types of models to use, the question is still too broad to be tackled: networks of interacting neurons defined by simple equations can have diverse behaviors depending on coupling and other parameters. Some of these behaviors are direct consequence of parameter choices; others are emergent, that is, they occur as a result of the dynamical interaction among neurons. There is no such thing as “typical” network behavior.

To select representative network models in a meaningful way, it was necessary to first identify the issues of interest. In our case, the most salient features of our “detailed” models that are not present in reduced models are correlations in subthreshold and spiking activity that emerge from neuronal interactions. Rate models do not treat individual neurons as entities, and do not therefore have the capacity to describe such correlations. This prompted us to look at not a single network model but a collection of networks with different amounts of correlations, using as a starting point a network that mimics the realistic model of the visual cortex in [7].

There is an earlier paper that had a similar goal as ours, namely [12], which compared networks of integrate-and-fire neurons with corresponding mean field models. They observed, as we did, that the degree of synchrony mattered. An important difference between the present paper and [12] is that we sought to identify the underlying mechanisms that led to discrepancies between network and reduced models. To our knowledge this is the first time such an analysis has been carried out.

The organization of this paper is as follows: In Section 1, we introduce a class of stochastic models of interacting neurons. These will be our “detailed” models. A mathematical treatment of these models is given in Section 2; this section can be skipped if the reader so chooses. In Section 3, we produce some network models with different degrees of synchrony, to be used for comparison with reduced models. In Section 4, we considered reduced models defined by simple ODEs, and in Section 5, we modeled fluctuations in membrane potential as random-walks.

1. A STOCHASTIC MODEL OF INTERACTING NEURONS

In this section, we introduce a stochastic model of interacting neurons representing a local population in the cerebral cortex. Though not intended to depict any specific part of the brain, this model has some of the features of realistic cortical models. Importantly, the dynamics are driven by neuronal interactions, with all the attendant correlated spiking behaviors that emerge as a result of these interactions. We have elected to use a stochastic model because with the aid of ergodicity, firing rates are represented simply and convergence is fast. The model presented here will be used in the rest of this paper to evaluate the performance of reduced models that are much simpler.

1.1. Model description. We consider a population of neurons connected by local circuitry, such as neurons in an orientation domain of one layer of the primary visual cortex. We assume that this population contains N_E excitatory (E) neurons and N_I inhibitory (I) neurons, which are sparsely and homogeneously connected. The following assumptions are made in order to formulate a simple Markov process that describes the spiking activity of this population.

- (1) We assume for simplicity that the membrane potential of a neuron takes only finitely many discrete values.
- (2) Each neuron receives synaptic input from an external source in the form of Poisson kicks; these kicks are independent from neuron to neuron.
- (3) When the membrane potential of a neuron reaches a certain threshold, the neuron spikes, after which it goes to a refractory state and remains there for an exponentially distributed random time.
- (4) Every time an E (respectively I) neuron in the population spikes:
 - (a) a random set of postsynaptic neurons is chosen;
 - (b) the membrane potential of each chosen postsynaptic neuron goes up (respectively down) after an exponentially distributed random time.

More precisely, we assume that in our population there are N_E excitatory neurons, labeled $1, 2, \dots, N_E$, and N_I inhibitory neurons, labeled $N_E+1, N_E+2, \dots, N_E+N_I$. The membrane potential of neuron i , denoted V_i , takes values in

$$\Gamma := \{-M_r, -M_r + 1, \dots, -1, 0, 1, 2, \dots, M\} \cup \{\mathcal{R}\} .$$

Here $M, M_r \in \mathbb{Z}^+$; M represents the threshold for spiking, $-M_r$ the inhibitory reversal potential, and \mathcal{R} the refractory state. When V_i reaches M , the neuron is said to *spike*, and V_i is instantaneously set to \mathcal{R} , where it remains for a duration given by an exponential random variable with mean $\tau_{\mathcal{R}} > 0$. When V_i leaves \mathcal{R} , it goes to 0.

We describe first the effects of the “external drive”, external in the sense that this input comes from outside of the population in question; for example it can be thought of as coming from a region of cortex closer to sensory input. This input is delivered in the form of impulsive kicks, arriving at random (Poissonian) times, the Poisson processes being independent from neuron to neuron. For simplicity, we assume there are two parameters, $\lambda^E, \lambda^I > 0$, representing the rates of the Poisson kicks to the E and I neurons in the population. These rates are low in background; they increase with the strength of the stimulation. When a kick arrives and $V_i \neq \mathcal{R}$, V_i jumps up by 1, until it reaches M , at which time the neuron spikes. Kicks received by neuron i when $V_i = \mathcal{R}$ have no effect.

Each neuron also receives synaptic input from within the population. We assume that an excitatory kick received by a neuron “takes effect” (the meaning of which will be made precise momentarily) at a random time after its arrival. This delay is given by an exponential random variable with mean τ^E ; it is independent from spike to spike and from neuron to neuron. Similarly, an inhibitory kick received takes effect after a random time with mean τ^I . We let H_i^E denote the number of

E-kicks received by neuron i that has not yet taken effect, and let H_i^I denote the corresponding number of I-kicks. That is to say, every time an E-kick is received by neuron i , H_i^E goes up by 1; every time an E-kick received by neurons i takes effect, H_i^E goes down by 1, and so on. The state of neuron i at any one moment in time is then described by the triplet (V_i, H_i^E, H_i^I) . We will refer to H_i^E and H_i^I as the numbers of kicks “in play”; these two numbers may be viewed as stand-ins for the E and I-conductances of neuron i .

We now explain what it means for an E or I-kick to take effect. Each E or I-kick received by neuron i carries with it an (independent) exponential clock as discussed above. When this clock rings, what happens depends on whether or not $V_i = \mathcal{R}$. If $V_i = \mathcal{R}$, then V_i is unchanged. If $V_i \neq \mathcal{R}$, then V_i is modified instantaneously according to the numbers $S_{Q,Q'}$, $Q, Q' \in \{E, I\}$, where $S_{Q,Q'}$ denotes the synaptic coupling when a neuron of type Q' synapses on a neuron of type Q . In the case of an I-kick, this modification also depends on V_i .

Here is how V_i is modified in the case of an E-kick, i.e., when $Q' = E$: Assume first that the numbers $S_{Q,Q'}$ are nonnegative integers. When an E-neuron spikes and it synapses on neuron i , V_i jumps up by S_{EE} if i is an E-neuron, by S_{IE} if i is an I-neuron; and if the jump takes V_i to an integer $\geq M$, it simply goes to \mathcal{R} . For non-integer values of $S_{Q,Q'}$, let $p = \lfloor S_{Q,Q'} \rfloor$ be the greatest integer less than or equal to $S_{Q,Q'}$. Then $S_{Q,Q'} = p + u$ where u be a Bernoulli random variable taking values in $\{0, 1\}$ with $\mathbb{P}[u = 1] = S_{Q,Q'} - p$ independent of all other random variables in the model.

When I-spikes take effect, the rule is analogous to that for E-spikes, with the following exception: V_i jumps down instead of up by an amount proportional to $V_i + M_r$, where $-M_r$ is the reversal potential for I-currents. The numbers $S_{Q,Q'}$ are assumed to be positive, and for definiteness, let us declare $S_{Q,I}$ to be the size of the jump at $V_i = M$, so that in general, the size of the jump is

$$S_{Q,I}(V_i) := (V_i + M_r)/(M + M_r) * S_{Q,I}.$$

We remark that we have incorporated into the numbers $S_{Q,Q'}$ the changes in *current* in the postsynaptic neuron. We have assumed that E-currents are independent of the membrane potential of the postsynaptic neuron, which is not unreasonable since the reversal potential for excitatory current is quite large ($> 4M$ in our setup). Changes in I-current are more sensitive to membrane potential, and that is reflected in the formula above.

It remains to stipulate the “connectivity” of the network, i.e., the set of neurons postsynaptic to each neuron. We assume for simplicity that connectivity in our model is random and time-dependent, so that every time a neuron spikes, a random set of postsynaptic neurons is chosen anew (independently of history). More precisely, for $Q, Q' \in \{E, I\}$, we let $P_{Q,Q'} \in [0, 1]$ be the probability that a neuron of type Q is postsynaptic when a neuron of type Q' spikes, and the set of postsynaptic neurons is determined by a coin flip with these probabilities following each spike. We do not pretend this assumption is realistic; in the real brain connectivities between neurons are fixed and far from random. But unlike longer range projections, which tend to target specific regions or even neurons, exact connectivities within

local populations are not known to be important. This is a rationale behind our assumption of random postsynaptic neurons. Another is that this assumption simplifies the analysis considerably. In particular, it makes the behaviors of all neurons in the E-population, respectively the I-population, statistically indistinguishable.

This completes our description of the model.

1.2. Parameters used in numerical results. There is an analytical and a numerical part to our results. Our rigorous results apply to all parameter choices that satisfy the hypotheses in the theorems or propositions. We give a sense here of the parameters we use in simulations: We generally take N_E to range from 300 to 1000, and $N_I = \frac{1}{3}N_E$, as is typically the case in local populations in the real cortex. We set $M = 100$, $M_r = 66$, the ratio of M_r to M reflecting biologically realistic ranges of membrane potentials. We fix $P_{EE} = 0.15$, $P_{IE} = P_{EI} = 0.5$ and $P_{II} = 0.4$, these numbers chosen to resemble the usual connectivities in networks such as those in the visual cortex. There is less experimental guidance for the synaptic couplings $S_{Q,Q'}$; we take them to be 2 – 6, out of the 100 units between reset and threshold (cf $S_{EE} = 5$ means it takes 20 consecutive E-kicks to drive a neuron from $V_i = 0$ to $V_i = M$). We set $\tau_R = 2 - 3$ (ms), consistent with usual estimates for refractory periods, and set τ^E and τ^I to be a few ms, with $\tau^E < \tau^I$, as AMPA is known to act faster than GABA and both act within milliseconds. We will, on occasion, deliberately choose parameters that are a little unbiological to make a point. Finally, the Poisson rates of the external drive, λ^E, λ^I will be varied as we study the model's responses to drives of various strengths.

Readers who wish to bypass the technical mathematics pertaining to the class of models described above can proceed without difficulty to Section 3.

2. THEORETICAL RESULTS AND PROOFS

Some basic results for the model presented in Sect. 1.1 are stated in Sect. 2.1, and their proofs are given in Sect. 2.3, after a brief review of probabilistic preliminaries.

2.1. Statement of results. The model described above is that of a Markov jump process Φ_t on a countable state space

$$\mathbf{X} = (\Gamma \times \mathbb{Z}_+ \times \mathbb{Z}_+)^{N_E + N_I},$$

as the state of neuron i is given by the triplet (V_i, H_i^E, H_i^I) where $V_i \in \Gamma$ and $H_i^E, H_i^I \in \mathbb{Z}_+ := \{0, 1, 2, \dots\}$. We assume the paths of Φ_t are càdlàg. The transition probabilities of Φ_t are denoted by $P^t(\mathbf{x}, \mathbf{y})$, i.e.,

$$P^t(\mathbf{x}, \mathbf{y}) = \mathbb{P}[\Phi_t = \mathbf{y} \mid \Phi_0 = \mathbf{x}].$$

The left operator of P^t acting on a probability distribution μ is

$$\mu P^t(\mathbf{x}) = \sum_{\mathbf{y} \in \mathbf{X}} \mu(\mathbf{y}) P^t(\mathbf{y}, \mathbf{x}).$$

The right operator of P^t acting on an observable $\xi : \mathbf{X} \rightarrow \mathbb{R}$ is

$$P^t \xi(\mathbf{x}) = \sum_{\mathbf{y} \in \mathbf{X}} P^t(\mathbf{x}, \mathbf{y}) \xi(\mathbf{y}).$$

Our first result pertains to the existence and uniqueness, hence ergodicity, of invariant measure for the Markov chain Φ_t . Notice that as H_i^E and H_i^I can take arbitrarily large values, the state space for Φ_t is noncompact, and such Markov chains need not possess invariant probabilities in general.

For $U : \mathbf{X} \mapsto (0, \infty)$, we define the U -weighted total variation norm of a signed measure μ on $\mathcal{B}(\mathbf{X})$, the Borel σ -algebra of \mathbf{X} , to be

$$\|\mu\|_U = \sum_{\mathbf{x} \in \mathbf{X}} U(\mathbf{x}) |\mu(\mathbf{x})|,$$

and let

$$L_U(\mathbf{X}) = \{\mu \text{ on } \mathcal{B}(\mathbf{X}) \mid \|\mu\|_U < \infty\}.$$

To state the main result, we need the following definitions. For each state $\mathbf{x} \in \mathbf{X}$, we let

$$H^E(\mathbf{x}) = \sum_{i=1}^{N_E+N_I} H_i^E \quad \text{and} \quad H^I(\mathbf{x}) = \sum_{i=1}^{N_E+N_I} H_i^I$$

be the total number of E-kicks and I-kicks in play.

Theorem 2.1. *The Markov chain Φ_t admits a unique invariant probability measure $\pi \in L_U(\mathbf{X})$ where*

$$U(\mathbf{x}) = H^E(\mathbf{x}) + H^I(\mathbf{x}) + 1.$$

This stationary measure is ergodic with exponential convergence to equilibrium, equivalently exponential decay of time correlations. More precisely, there exist constants $C_1, C_2 > 0$ and $r \in (0, 1)$, such that

(a) *for any initial distribution $\mu \in L_U(\mathbf{X})$,*

$$\|\mu P^t - \pi\|_U \leq C_1 r^t \|\mu - \pi\|_U;$$

(b) *for any observable ξ with $\|\xi\|_U < \infty$,*

$$\|P^t \xi - \pi(\xi)\|_U \leq C_2 r^t \|\xi - \pi(\xi)\|_U,$$

where

$$\pi(\xi) = \sum_{\mathbf{x} \in \mathbf{X}} \pi(\mathbf{x}) \xi(\mathbf{x}).$$

For $T > 0$, we let $N_i(T)$ denote the number of times neuron i spikes on the time interval $[0, T]$. Equivalently, $N_i(T)$ is the random variable that counts the number of visits of V_i to state M (or to state \mathcal{R}). Then the *mean firing rate* of neuron i is defined to be

$$\text{fr}(i) := \lim_{T \rightarrow \infty} \frac{1}{T} \mathbb{E}_\pi[N_i(T)] = \mathbb{E}_\pi[N_i(1)]$$

where \mathbb{E}_π is the expectation with respect to the invariant probability π given by Theorem 2.1. As defined, $\text{fr}(i)$ is a number in $[0, \infty]$, and the second equality follows

from the invariance of π . Since all E-neurons have the same firing rates, and the same is true for all I-neurons, we denote the mean E- and I-firing rates of Φ_t by \bar{F}_E and \bar{F}_I respectively.

In the next corollary, we assume $S_{Q,Q'}$ are integers, and leave the formulation of results for noninteger values of $S_{Q,Q'}$ to the reader. For each state $\mathbf{x} \in \mathbf{X}$, we define

$$F_E^{\text{tot}}(\mathbf{x}) = \sum_{i=1}^{N_E} \left(\frac{1}{\tau^E} H_i^E \cdot \mathbf{1}_{\{V_i \geq M - S_{EE}\}}(\mathbf{x}) + \lambda^E \cdot \mathbf{1}_{\{V_i = M-1\}}(\mathbf{x}) \right),$$

$$F_I^{\text{tot}}(\mathbf{x}) = \sum_{i=N_E+1}^{N_E+N_I} \left(\frac{1}{\tau^E} H_i^E \cdot \mathbf{1}_{\{V_i \geq M - S_{IE}\}}(\mathbf{x}) + \lambda^I \cdot \mathbf{1}_{\{V_i = M-1\}}(\mathbf{x}) \right).$$

Corollary 2.2. *The firing rates $\bar{F}_E, \bar{F}_I < \infty$ and satisfy*

$$\bar{F}_E = \frac{1}{N_E} \sum_{\mathbf{x} \in \mathbf{X}} F_E^{\text{tot}}(\mathbf{x}) \pi(\mathbf{x}) \quad \text{and} \quad \bar{F}_I = \frac{1}{N_I} \sum_{\mathbf{x} \in \mathbf{X}} F_I^{\text{tot}}(\mathbf{x}) \pi(\mathbf{x}).$$

2.2. Probabilistic Preliminaries. We review the following general results on geometric ergodicity. Let Ψ_n be a Markov chain on a countable state space (X, \mathcal{B}) with transition kernels $\mathcal{P}(x, \cdot)$, and let $W : X \rightarrow [1, \infty)$. Consider the following conditions:

- (a) There exist constants $K \geq 0$ and $\gamma \in (0, 1)$ such that

$$(\mathcal{P}W)(x) \leq \gamma W(x) + K$$

for all $x \in X$.

- (b) There exists a constant $\alpha \in (0, 1)$ and a probability measure ν so that

$$\inf_{x \in C} \mathcal{P}(x, \cdot) \geq \alpha \nu(\cdot),$$

with $C = \{x \in X \mid W(x) \leq R\}$ for some $R > 2K(1 - \gamma)$, where K and γ are from (a).

The following was first proved in [18]. The version we use is proved in [13].

Theorem 2.3. *Assume (a) and (b). Then Ψ_n admits a unique invariant measure $\pi \in L_W(X)$. In addition, there exist constants $C, C' > 0$ and $r \in (0, 1)$ such that (ii) for all $\mu, \nu \in L_W(X)$,*

$$\|\mu \mathcal{P}^n - \nu \mathcal{P}^n\|_W \leq C r^n \|\mu - \nu\|_W,$$

and (i) for all ξ with $\|\xi\|_W < \infty$,

$$\|\mathcal{P}^n \xi - \pi(\xi)\|_W \leq C' r^n \|\xi - \pi(\xi)\|_W.$$

2.3. Proof of Theorem 2.1 and Corollary 2.2. For a step size $h > 0$, we define the time- h sample chain as $\Phi_n^h = \Phi_{nh}$, and drop the superscript h when it leads to no confusion. We first show for this discrete-time chain that $U(\mathbf{x}) = H^E(\mathbf{x}) + H^I(\mathbf{x}) + 1$ is a natural Lyapunov function that satisfies conditions (a) and (b) in the previous subsection.

Lemma 2.4. *For $h > 0$ sufficiently small, there exist constants $K > 0$ and $\gamma \in (0, 1)$, such that*

$$P^h U \leq \gamma U + K.$$

Intuitively, this is true because on a short time interval $(0, h)$, U decreases at a rate proportional to $H^E + H^I$ as kicks received prior to time 0 take effect, while it can increase at most by a fixed constant related to $N_E + N_I$ due to the presence of the refractory period.

Proof. We have

$$P^h U(\mathbf{x}) = \mathbb{E}_{\mathbf{x}}[U(\Phi_h)] \leq U(\mathbf{x}) - \mathbb{E}_{\mathbf{x}}[N_{out}] + \mathbb{E}_{\mathbf{x}}[N_{in}],$$

where N_{out} is the number of kicks from $H^E + H^I$ that takes effect on $(0, h]$, and N_{in} is the number of new spikes produced during the time period $(0, h]$.

To estimate N_{out} , recall that the clocks associated with each of the $H^E + H^I$ kicks are independent, with each E-kick taking effect on $(0, h]$ with probability $(1 - e^{-h/\tau^E})$ and each I-kick taking effect on $(0, h]$ with probability $(1 - e^{-h/\tau^I})$. This gives

$$\mathbb{E}_{\mathbf{x}}[N_{out}] \geq (H^E + H^I)(1 - e^{-h/\max\{\tau^E, \tau^I\}}) \geq \frac{1}{2 \max\{\tau^E, \tau^I\}} h U(\mathbf{x})$$

for h sufficiently small.

To estimate N_{in} , consider neuron i , and let f_i be the number of spikes generated by neuron i during the time period $(0, h]$. Since after each spike neuron i spends an exponential time with mean $\tau_{\mathcal{R}}$ in state \mathcal{R} , we have

$$\mathbb{E}_{\mathbf{x}}[f_i] \leq 1 + \mathbb{E}[\text{Poisson distribution with parameter } h/\tau_{\mathcal{R}}] = 1 + h/\tau_{\mathcal{R}}.$$

Hence

$$\mathbb{E}_{\mathbf{x}}[N_{in}] \leq (N_E + N_I)(1 + h/\tau_{\mathcal{R}}).$$

The proof is completed by letting

$$\gamma = 1 - h/(2 \max\{\tau^E, \tau^I\}) \quad \text{and} \quad K = (N_E + N_I)(1 + h/\tau_{\mathcal{R}}).$$

□

For $b \in \mathbb{R}$, let

$$C_b = \{\mathbf{x} \in \mathbf{X} \mid H^E(\mathbf{x}) + H^I(\mathbf{x}) \leq b\}.$$

Lemma 2.5. *Let \mathbf{x}_0 be the state that $H^E = H^I = 0$ and $V_i = \mathcal{R}$ for all i . Then for any $h > 0$, there exists a constant c depending on b and h such that for all $\mathbf{x} \in C_b$,*

$$P^h(\mathbf{x}, \mathbf{x}_0) > c.$$

Proof. It is sufficient to construct, for each $\mathbf{x} \in C_b$, a sample path that goes from \mathbf{x} to \mathbf{x}_0 with a uniform lower bound on its probability. Consider the following sequence of events.

- (i) A sequence of Poisson kicks increases each V_i to the threshold value M , hence puts $V_i = \mathcal{R}$, by time $t = h/2$; once in \mathcal{R} , V_i remains there through time $t = h$. No kick in play takes effect on $[0, h/2]$.
- (ii) All kicks in play at time $h/2$ take effect on $(h/2, h]$, but that has no effect as all V_i are in \mathcal{R} .

To prove that the events above occur with a positive probability bounded from below, observe that in the scenario described, the number of kicks in play never exceeds $b + N_E + N_I$, hence only a finite number of conditions are imposed. \square

Lemmas 2.4 and 2.5 together imply Theorem 2.1.

Proof of Theorem 2.1. Choose step size h as in Lemma 2.4. It follows from Lemma 2.4 and 2.5 that the assumptions in Theorem 2.3 are satisfied. Therefore, the discrete-time chain Φ^h admits a unique invariant probability measure π_h in $L_U(\mathbf{X})$.

We will show that π_h is invariant under Φ_t for any $t > 0$. This is because Φ_t satisfies the ‘‘continuity at zero’’ condition, meaning for any probability measure μ on \mathbf{X} ,

$$\lim_{t \rightarrow 0} \|\mu P^t - \mu\|_{TV} = 0.$$

To see this, let $\epsilon > 0$ be an arbitrary small number. Since μ is finite, there exists a finite set $A \subset \mathbf{X}$ such that $\mu(A) > 1 - \epsilon/4$. By the definition of A , clock rates for initial values in A are uniformly bounded. Therefore, one can find a sufficiently small $\delta > 0$, such that $\mathbb{P}[\text{no clock rings on } [0, \delta]] \geq 1 - \epsilon/4$. For any set $U \subset \mathbf{X}$, we have

$$\begin{aligned} (\mu P^\delta)(U) &= \sum_{\mathbf{x} \in \mathbf{X}} P^\delta(\mathbf{x}, U) \mu(\mathbf{x}) \\ &= \sum_{\mathbf{x} \in A \cap U} P^\delta(\mathbf{x}, U) \mu(\mathbf{x}) + \sum_{\mathbf{x} \in A - U} P^\delta(\mathbf{x}, U) \mu(\mathbf{x}) + \sum_{\mathbf{x} \in A^c} P^\delta(\mathbf{x}, U) \mu(\mathbf{x}) \\ &= \mu(A \cap U) - a_1 + a_2 + a_3, \end{aligned}$$

where

$$\begin{aligned} a_1 &= \sum_{\mathbf{x} \in A \cap U} (1 - P^\delta(\mathbf{x}, U)) \mu(\mathbf{x}) \leq \frac{\epsilon}{4} \mu(A \cap U) \leq \frac{\epsilon}{4} \\ a_2 &= \sum_{\mathbf{x} \in A \setminus U} P^\delta(\mathbf{x}, U) \mu(\mathbf{x}) \leq \frac{\epsilon}{4} \mu(A \setminus U) \leq \frac{\epsilon}{4} \\ a_3 &= \sum_{\mathbf{x} \in A^c} \frac{\epsilon}{4} \mu(A \cap U) \leq \frac{\epsilon}{4} \leq \mu(A^c) \leq \frac{\epsilon}{4}. \end{aligned}$$

In addition we have $\mu(U) - \mu(A \cap U) \leq \mu(A^c) < \frac{\epsilon}{4}$. Hence

$$|(\mu P^\delta)(U) - \mu(U)| < \epsilon$$

for any $U \subset \mathbb{R}_+^N$. By the definition of the total variation norm, we have

$$\|\mu P^\delta - \mu\|_{TV} \leq \epsilon.$$

This implies the ‘‘continuity at zero’’ condition.

Notice that π_h is invariant for any $\Psi_n^{h_j/k}$, where $j, k \in \mathbb{Z}^+$ (Theorem 10.4.5 of [18]). Then without loss of generality, assume $t/h \notin \mathbb{Q}$. By the density of orbits in irrational rotations, there exists sequences $a_n, b_n \in \mathbb{Z}^+$ such that

$$d_n := t - \frac{a_n}{b_n}h \rightarrow 0$$

from right. Then

$$\pi_h P^t = \pi_h P^{\frac{a_n}{b_n}h} P^{d_n}.$$

Therefore,

$$\|\pi_h P^t - \pi_h\|_{TV} \leq \lim_{n \rightarrow \infty} \|\pi_h P^{d_n} - \pi_h\|_{TV} = 0$$

by the ‘‘continuity at zero’’ condition. Hence π_h is invariant with respect to P^t .

It remains to prove the exponential convergence for any $t > 0$. By Lemma 2.4, there exists B such that $P^t V \leq BV$ for all $t < h$. Let n be the largest integer that is smaller than t/h and let $d = t - hn$. Then we have

$$\begin{aligned} \|\mu P^t - \nu P^t\|_V &= \|(\mu P^d) P^{nh} - (\nu P^d) P^{hn}\|_V \\ &= Cr^n \cdot \|\mu P^d - \nu P^d\|_V \leq BCr^n \|\mu - \nu\|_V. \end{aligned}$$

Similarly,

$$\begin{aligned} \|P^t \xi - \pi(\xi)\|_V &= \|P^{nh}(P^d \xi) - P^{hn}(P^d \pi(\xi))\|_V \\ &= Cr^n \cdot \|P^d \xi - P^d \pi(\xi)\|_V \leq BCr^n \|\xi - \pi(\xi)\|_V. \end{aligned}$$

This completes the proof. \square

Proof of Corollary 2.2. As in the proof of Lemma 2.4, we have that for every \mathbf{x} ,

$$\mathbb{E}_{\mathbf{x}}[N_i(1)] \leq 1 + \mathbb{E}[\text{Poisson distribution with parameter } 1/\tau_{\mathcal{R}}] = 1 + 1/\tau_{\mathcal{R}}.$$

Thus $\text{fr}(i) = \mathbb{E}_{\pi}[N_i(1)] < \infty$.

Now for an infinitesimally small $h > 0$, the probability that a spike is fired by some E-neuron on the time interval $[0, h]$ starting from \mathbf{x} is $F_E^{\text{tot}}(\mathbf{x}) \cdot h$. Thus starting from $\mathbf{x} = \Phi_0$,

$$\bar{F}_E = \frac{1}{N_E} \cdot \lim_{T \rightarrow \infty} \frac{1}{T} \int_0^T F_E^{\text{tot}}(\Phi_t) dt$$

which by the Ergodic Theorem is equal to the asserted quantity. The same argument applies to \bar{F}_I . \square

3. THREE POPULATIONS WITH DIFFERENT DEGREES OF SYNCHRONY

One of the reasons why a rigorous analysis of the dynamics of populations of interacting neurons is challenging is that these interactions produce correlations in temporal dynamics, and coordinated dynamical events in turn influence how the neurons interact. Correlations in neuronal dynamics clearly exist in the real brain: LFP oscillations in the gamma band, which are found in many parts of cortex, are likely the result of self-organized, coordinated subthreshold activity. A related phenomenon is clustering or partial synchronization of spikes. An extreme version of it involving full-population spikes is known as PING [3]. Milder, more subtle, forms of partial synchronization that appear to be more consistent with experimental observations [15] in cortex were later identified in the modeling work of [22] and studied in [21, 9]; similar phenomena were reproduced in the realistic models in [7] and [8].

In other developments in neuroscience, many reduced models (e.g. [24, 25, 17, 2, 19, 14]) have been proposed, giving rise to simpler ways to deduce the firing rates of local populations. As discussed in the Introduction, one of the aims of this paper is to investigate the accuracy of these predictions, and the degree to which they may (or may not) be affected by emergent correlations in network activity. In the rest of this paper, we will make believe that the stochastic model presented in Sect. 1.1 is “real”, and its firing rates will be compared to those given by some of the simplest reduced models.

While our intentions are clear, a question arises immediately with regard to which parameters that define the network models in Sect. 1.1 to use. Numerical exploration tells us quickly that there is no such thing as a typical network model, and that different parameter choices can lead to a wide range of dynamical behaviors. Obviously we cannot exhaust all possibilities in a high dimensional parameter space. Since our main concern is the effect of correlated spiking, we will introduce in this section three examples of network models exhibiting different degrees of correlated spiking or partial synchrony, and use them for illustration in the next section.

3.1. Three example networks. We introduce here three models of the type described in Sect. 1.1, with identical parameters except for τ^E and τ^I , the expected time between the occurrence of a spike and when it takes effect. As we will see, different choices of these values will lead to different degrees of synchrony.

We first give the parameters common to all three models: N_E and N_I , the numbers of E and I neurons in the population, are 300 and 100 respectively. The connectivities $P_{QQ'}$ are as in Sect. 2.1, namely $P_{EE} = 0.15$, $P_{IE} = P_{EI} = 0.5$ and $P_{II} = 0.4$. The synaptic weights $S_{QQ'}$ are as follows: $S_{EE} = 5$, $S_{IE} = 2$, and $S_{EI} = S_{II} = 4.91$ (recall that this corresponds to coupling weights when V_i , the membrane potential of the postsynaptic neuron, is at threshold, i.e. at $V_i = 100$). The expected time to stay in the refractory state, \mathcal{R} , is 2.5 ms, and the external drive rates to E and I neurons will be taken to be equal, i.e., $\lambda^E = \lambda^I$, and a range of values of the drive will be considered.

The parameters above, for the most part, are similar to those used in the realistic models of visual cortex [7]. From [8], we learned also that varying the rise and decay times of E and I conductances, especially the relation between the two, is a very effective way to change the degree of synchrony of a local population. We now use this technique to produce the following three examples:

- (1) The “**homogeneous**” network, abbreviated as “**Hom**” in the figures:

$$\tau^{EE} = 4, \quad \tau^{IE} = 1.2, \quad \tau^I = 4.5 \quad (\text{in ms})$$

- (2) The “**regular**” network, abbreviated as “**Reg**” in the figures:

$$\tau^{EE} = 2.0, \quad \tau^{IE} = 1.2, \quad \tau^I = 4.5 \quad (\text{in ms})$$

- (3) The “**synchronized**” network, abbreviated as “**Sync**” in the figures:

$$\tau^{EE} = 1.3, \quad \tau^{IE} = 0.95, \quad \tau^I = 4.5 \quad (\text{in ms})$$

Instead of τ^E , we have used here τ^{EE} and τ^{IE} to denote the expected times between the occurrence of an E-spike and when it takes effect in E, respectively I, neurons. These numbers are roughly consistent with biological values: $\tau^I > \tau^{EE}$, τ^{IE} is consistent with the fact that GABA acts more slowly than AMPA, and $\tau^{EE} > \tau^{IE}$ is consistent with the fact that E-spikes can synapse on dendrites of E-neurons, taking a bit longer for its effect to reach the soma, while they synapse directly on the soma of I-cells. That aside, there is nothing special about these choices, other than that they produce the distinct degrees of synchrony that we would like to have.

Figure 1 shows the E- and I-firing rates of the three networks above in response to a range of drives of magnitude $\lambda = \lambda^E = \lambda^I$ spikes/sec. Both firing rates increase monotonically as a function of drive. We think of $\lambda \sim 1000$ spikes/sec as low drive, or spontaneous activity, and $\lambda \geq 6000$ spikes/sec as strong drive.

3.2. Statistics of the “Hom”, “Reg” and “Sync” networks. Here we present more detailed information on the three networks defined in the last subsection, focusing on their responses to relatively strong drive, at $\lambda = 7000$ spikes/sec. Fig 2 shows, for each network, spike rasters, summed spike plots, and correlation diagrams.

The raster-plots are self-explanatory. Clearly visible in the rasters of the Reg and Synch networks are coordinated spiking that emulate gamma band oscillations (at 30-90 Hz) in the real cortex [15]. These spiking events are entirely emergent, or self-organized, in the sense that there is nothing built into the network architecture or dynamics that lead directly to these spiking events. Comparing the frequency of these events with mean E-firing rate (given above the rasters), one sees that most E-neurons do not participate in all spiking events.

The summed spike plots give the fractions of the E-population spiking in 5-ms time bins. Though they show the same behaviors as the rasters, we have included these plots because rasters can be deceiving when used to depict the spiking activity of hundreds of neurons: what appear to be population spikes may in fact involve fewer neurons than the rasters suggest. For the Sync network, one sees from the summed spike plots that most spiking events do not involve the entire population, even though the rasters may give an impression to the contrary. As for the Reg

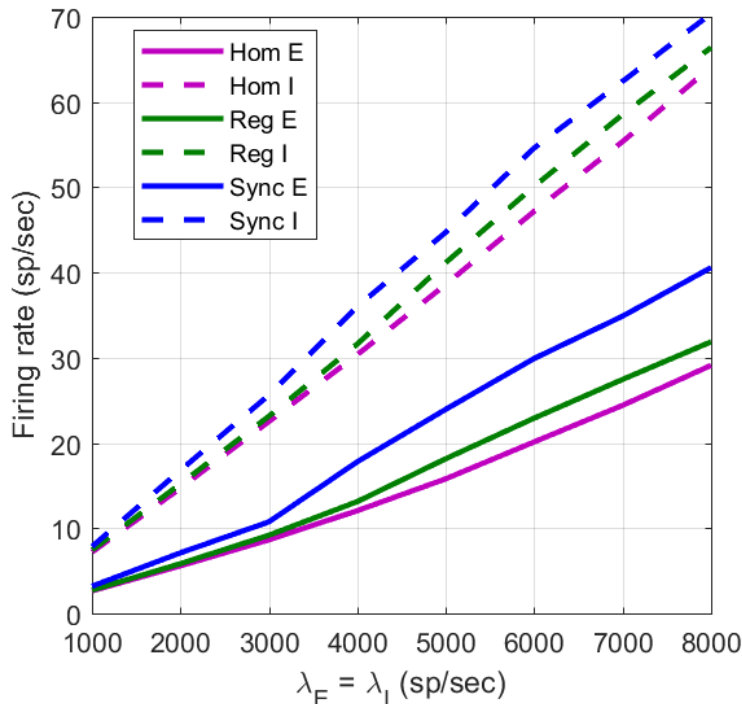


FIGURE 1. **Firing rates of three example networks in response to increasing drive.** In the x -axis, $\lambda = \lambda^E = \lambda^I$ is external drive. The graphs labeled “Hom”, “Reg” and “Sync” give the firing rates of the corresponding networks.

network, Fig 2 shows that the larger spiking events usually involve no more than 30 – 40% of the population. Nor do identical fractions of neurons spike in each 5 ms bin in the Hom network: there is some amount of synchronization that is entirely emergent, natural and hard to avoid.

The correlation diagrams describe not correlations between pairs of neurons but how the spiking of individual neurons are correlated to that of the rest of the population. We describe precisely what is plotted in, for example, the second histogram from the left, labeled “Conditioned on E at $t = 0$ ” with an “I” in the box. Here we run the network for 10-20 seconds. Each time an E-neuron spikes, we record all the I-spikes fired within 15 ms of its occurrence, both before and after, computing the fraction of the I-population spiking in each 1-ms time bin on this time interval. This is then averaged over all E-spikes that occur during the simulation. The other three plots are interpreted analogously. A comparison of these plots for the three networks confirms the increasing amounts of correlated spiking, or partial synchrony, that are clearly visible in the rasters as we go from the Hom to the Sync network.

Analysis. We have presented three example networks defined by essentially the same parameters yet exhibiting remarkably dissimilar spiking patterns, from very

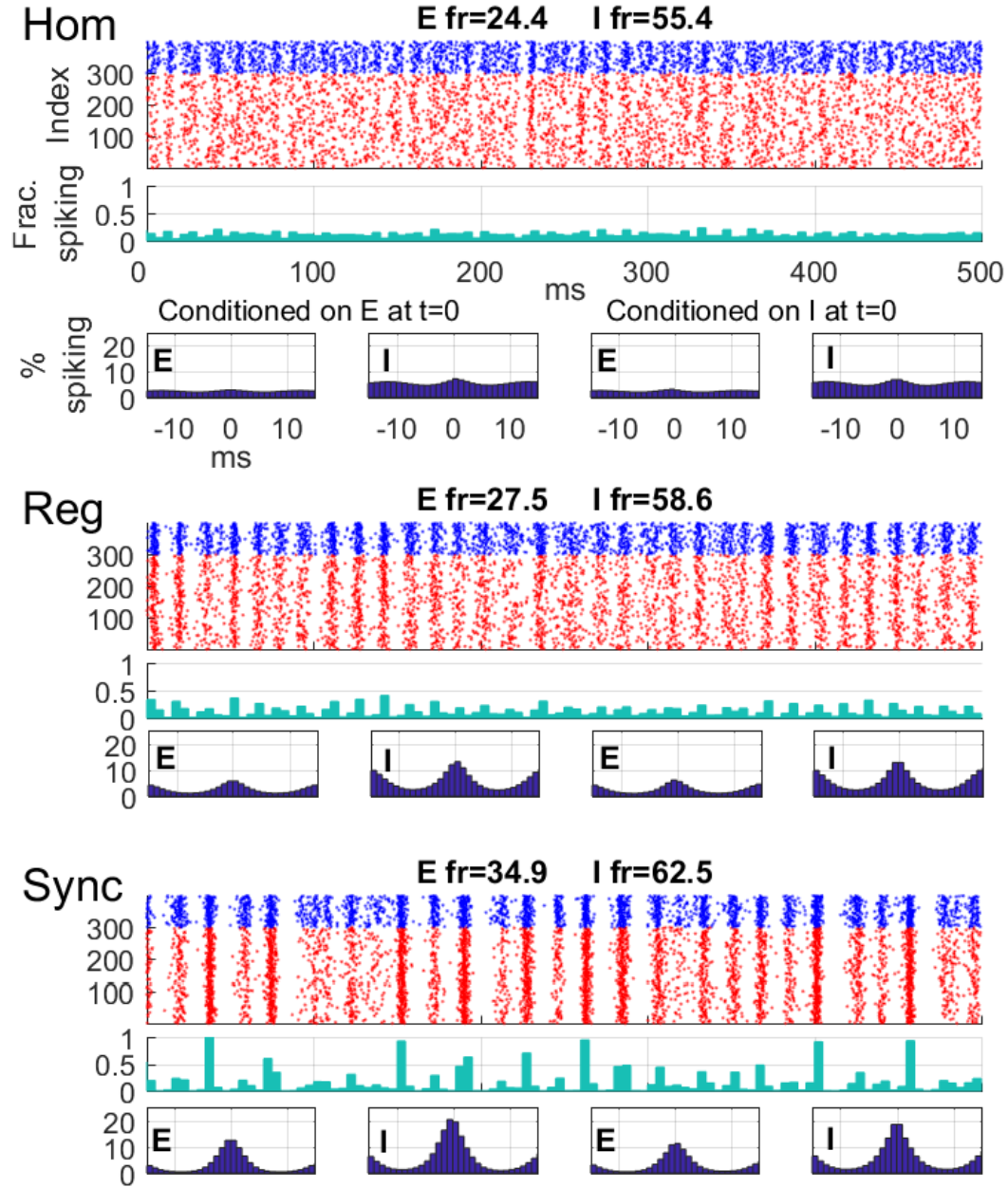


FIGURE 2. Statistics of the Hom, Reg and Sync networks: All statistics are collected in response to a strong drive of $\lambda^E = \lambda^I = 7000$ spikes/sec. For each network we show in the top panel rasters (E-neurons in red, I-neurons in blue) over a 1/2 sec time interval; mean firing rates are shown above the rasters. In the middle panel are corresponding summed spike plots for E-neurons, showing the percentage of the E-population spiking in each 5 ms window. Below the summed spike plots are correlation diagrams: a histogram labeled “X conditioned on Y at $t = 0$ ”, $X, Y = E, I$, shows the percentage of the X-population spiking on 1 ms windows on the time interval $t \in [-15, 15]$ ms conditioned on a Y-spike occurring at time $t = 0$. Labels for the Reg and Sync networks, which are omitted, are to be read as identical to those for the Hom network.

homogeneous to strongly synchronized. The only differences in network parameters are τ^E and τ^I , which describe how long after one neuron synapses on another before the effect of the spike is fully felt. Even here, the differences are subtle: the homogeneous and regular networks differ only in τ^{EE} and by only 2 ms, while all three τ -parameters differ by < 1 ms between the regular and synchronized networks.

Two points here are of note. First, when under drive, the most salient kind of correlations among neurons in the model are semi-regular bursts of elevated spiking occurring with frequencies in the gamma band (not to suggest that these are the only correlations). Second, our simulations confirm that small changes in τ^E and τ^I , intended to represent how AMPA and GABA affect conductance properties in the postsynaptic neuron in the real brain, have a strong impact on the amount of correlated spiking or degree of synchronization in the local population.

The mechanism behind gamma band oscillations has been much studied. An extreme form of it involving full population spikes, called PING, was first described in [3]. Milder and more realistic forms producing spectral power densities much closer to data were studied in [21, 9] and [8]. We refer the reader to these papers for a more detailed discussion. Very briefly, these rhythms occur as a result of recurrent excitation and the fact that the time course for GABA is generally a few ms slower than that of AMPA, allowing some fraction of the E- and I-population to spike before a sufficient amount of GABA is released to curb the spiking activity.

Finally, to be clear, we do not claim that the examples above are representative of all network models. If anything, they illustrate that neuronal interactions can produce a wide range of dynamical characteristics, and that these characteristics can depend on model parameters in subtle ways. But with partial synchronization being one of the most salient features of driven neuronal dynamics, these three examples allow us close-up looks into how reduced models perform when used to predict the dynamics of networks with different degrees of synchronization.

4. FIRING RATES: COMPARISON OF REDUCED AND NETWORK MODELS

Up until now, we have focused on models defined by populations of interacting neurons. We now turn to the use of reduced models to estimate their firing rates. Three very simple ODEs describing the evolution of membrane potential are proposed in Sect. 4.1. No novelty is claimed here with regard to these reduced models; many similar ideas for deducing firing rates by balancing one quantity or another have been proposed in the literature (see e.g. [24, 25, 17, 1, 2, 23, 19, 11, 4, 14, 6, 5, 20]). The reduced models we have selected for consideration were chosen for their simplicity, and the fact that they allow a direct comparison with the network models studied in Sections 1–3. Such a comparison is carried out in Sect. 4.2, followed by an analysis of the discrepancies.

4.1. Three reduced models and their firing rates. The models below will be referred to by their names in *italics* in later discussion.

(1) *Linear model.* In this first reduced model we regard the membrane potential v of each neuron as drifting upward at constant speed, i.e.,

$$(4.1) \quad \frac{dv}{dt} = F^+ - F^- , \quad \text{for } v \in [0, 1] .$$

Upon reaching 1, v is instantaneously reset to 0, and the climb starts immediately (with no refractory period). Here F^+ and F^- are the forces that drive v upward, respectively downward. They are connected to the quantities that describe the network models in Sect. 1.1 as follows: Let

$$(4.2) \quad \begin{aligned} C_{EE} &= N_E P_{EE} S_{EE} , & C_{IE} &= N_E P_{IE} S_{IE} , \\ C_{EI} &= N_I P_{EI} \hat{S}_{EI} , & C_{II} &= N_I P_{II} \hat{S}_{II} , \end{aligned}$$

where \hat{S}_{EI} and \hat{S}_{II} are to be taken to be the value of $S_{EI}(v)$ and $S_{II}(v)$ at $v = M/2 = 50$ in the model in Sect. 1.1. Then for E-neurons,

$$F^+ = \frac{1}{M} (f_E * C_{EE} + \lambda^E) \quad \text{and} \quad F^- = \frac{1}{M} f_I * C_{EI} ,$$

and for I-neurons,

$$F^+ = \frac{1}{M} (f_E * C_{IE} + \lambda^I) \quad \text{and} \quad F^- = \frac{1}{M} f_I * C_{II} .$$

Here f_E and f_I are to be thought of as mean E- and I-firing rates of the population.

The mean excitatory and inhibitory firing rates $f_E^{(1)}$ and $f_I^{(1)}$ of this reduced model are defined to be the values of f_E and f_I that satisfy the self-consistency condition that when these values are plugged into the equations above, they produce the same firing rates (the number of times per sec v in (4.1) reaches 1). They can be computed explicitly as follows:

Lemma 4.1. *The values $(f_E^{(1)}, f_I^{(1)})$ are uniquely defined and are given by the formulas below, provided the quantities on the right side are ≥ 0 :*

$$(4.3) \quad \begin{aligned} f_E^{(1)} &= \frac{\lambda^E (M + C_{II}) - \lambda^I C_{EI}}{(M - C_{EE})(M + C_{II}) + (C_{EI} C_{IE})} \\ f_I^{(1)} &= \frac{\lambda^I (M - C_{EE}) + \lambda^E C_{IE}}{(M - C_{EE})(M + C_{II}) + (C_{EI} C_{IE})} , \end{aligned}$$

With $\lambda^E = \lambda^I$ as we have done in Section 3, it is easy to see that $f_E^{(1)}$ and $f_I^{(1)}$ increase linearly as functions of drive.

(2) *Linear model with refractory.* This model is similar to the previous one, except for the presence of a (fixed) refractory period. That is to say, here

$$\frac{dv}{dt} = F^+ - F^- , \quad \text{for } v \in [0, 1] ,$$

except that every time v reaches 1 and is reset to 0, it remains there for a time interval of length τ_R before resuming its linear climb. See Fig 3A (second from left).

The mean E- and I-firing rates of this model, $(f_E^{(2)}, f_I^{(2)})$, are then given by the pair (f_E, f_I) satisfying the quadratic equations

$$(4.4) \quad M * f_E = (1 - \tau_{\mathcal{R}} f_E)(f_E * C_{EE} + \lambda^E - f_I * C_{EI})$$

$$(4.5) \quad M * f_I = (1 - \tau_{\mathcal{R}} f_E)(f_E * C_{IE} + \lambda^E - f_I * C_{II}) .$$

Theoretically, these equations can be solved analytically. From the first equation of (4.4), it is easy to see that

$$f_I = \frac{(1 - \tau_{\mathcal{R}} f_E)(C_{EE} f_E + \lambda^E) - M f_E}{C_{EI}(1 - \tau_{\mathcal{R}} f_E)} .$$

Putting f_I into the second equation of (4.4) and multiplying both sides by $(1 - \tau_{\mathcal{R}} f_E)^2$, we obtain a quartic equation for f_E of the form

$$A_0(\tau_{\mathcal{R}}) + A_1(\tau_{\mathcal{R}}) f_E + A_2(\tau_{\mathcal{R}}) f_E^2 + A_3(\tau_{\mathcal{R}}) f_E^3 + A_4(\tau_{\mathcal{R}}) f_E^4 = 0 ,$$

where $A_0 \sim A_4$ are polynomials in terms of $\tau_{\mathcal{R}}$. In particular, when $\tau_{\mathcal{R}} = 0$, this quartic equation reduces to the linear equation

$$(4.6) \quad [(M - C_{EE})(M + C_{II}) + (C_{EI} C_{IE})] f_E = \lambda^E (M + C_{II}) - \lambda^I C_{EI} ,$$

which produces $f_E^{(1)}$ in (4.3). It is well known that quartic equations have a root formula, which is unfortunately too complicated to be practical, but it gives the existence of solution to the quadratic system. In addition, for sufficiently small $\tau_{\mathcal{R}}$, the quartic equation is a small perturbation of equation (4.6). By the intermediate value theorem, it is easy to show that the quartic equation must admit a root that is close to $f_E^{(1)}$. We leave this elementary proof to the reader.

(3) The v -dependent model. Here v satisfies the same equation as before, except that S_{EI} and S_{II} depend on the distance of v to the reversal potential. To separate the effects of refractory and v -dependence of synaptic weights, let us assume for definiteness that there is no refractory period, that is to say, all is as in the linear model except for the following:

$$S_{EI}(v) = \frac{Mv + M_r}{M + M_r} * S_{EI} \quad \text{and} \quad S_{II}(v) = \frac{Mv + M_r}{M + M_r} * S_{II} .$$

For a given pair (f_E, f_I) , this gives us two first order linear ODEs

$$\frac{dv_E}{dt} = A_E - B_E v_E \quad \text{and} \quad \frac{dv_I}{dt} = A_I - B_I v_I ,$$

where A_E, A_I, B_E and B_I are easily computed from network parameters. We let t_E and t_I be the times v_E and v_I first reaches 1. Then the desired spike rates f_E and f_I should satisfy $f_E = t_E^{-1}$ and $f_I = t_I^{-1}$. That is, the firing rates $f_E^{(3)}$ and $f_I^{(3)}$ of this ODE model is the pair (f_E, f_I) that solves the two nonlinear equations

$$(4.7) \quad 1 = \frac{A_E}{B_E} (1 - e^{-B_E f_E^{-1}}) \quad , \quad 1 = \frac{A_I}{B_I} (1 - e^{-B_I f_I^{-1}}) .$$

These equations can be solved numerically.

Needless to say, one can also consider the combined effects of (2) and (3), to obtain a v -dependent model with refractory. In this case, equation (4.7) becomes

$$1 = \frac{A_E}{B_E}(1 - e^{-B_E(f_E^{-1} - \tau_R)}) \quad , \quad 1 = \frac{A_I}{B_I}(1 - e^{-B_I(f_I^{-1} - \tau_R)}) .$$

Firing rates for the first two reduced models are shown in Fig. 3B (left) using the parameters of the network models studied in Section 3. An immediate observation is that the model with refractory has higher firing rates, which may be somewhat counter-intuitive as the delay during refractory should, on the face of it, lead to lower firing rates. We have omitted the firing rates for the v -dependent model because they are ridiculously low (close to 0) and numerically unstable, and that requires an explanation as well. (Please ignore the plot with open circles for now.)

Analysis. The following is a heuristic explanation for $f_E^{(2)} > f_E^{(1)}$: As is usually the case, I-firing rate is significantly higher than E-firing rate in the models considered. With refractory, every time a neuron spikes, it “misses” some amount of the incoming drive, the net value of which is positive. Since the fraction of drive “missed” is proportional to the firing rate of a neuron in these models, the I-neuron “misses” a larger fraction of its drive than the E-neuron. This may cause the system to become more excited than in the case of no refractory. (In the argument above we have taken into account first order effects only, ignoring the secondary effect that higher E-firing will boost I-firing.)

With regard to the v -dependent model, our analysis shows that the root $(f_E^{(3)}, f_I^{(3)})$ is very sensitive with respect to small change of constants B_E and B_I . Small errors in B_E or B_I caused by the inhomogeneous arrival of spikes are dramatically amplified by the v -dependent model. As a result, the computed values are usually too low and not sufficiently reliable to be useful.

That begs the question then: why are firing rates in the network models so much higher than in the v -dependent model, and so robust? We believe stochastic fluctuations is the answer, and will study that in the next section.

4.2. Comparison of firing rates with network models. We now compare the firing rates of the network models in Sect. 3 and the reduced models in Sect. 4.1. The right panel of Fig 3B shows the firing rates of the two linear reduced models (with and without refractory) copied from the panel on the left and superimposed on the firing rates of the Hom, Reg and Sync models copied from Fig 1. We see immediately that the linear reduced model underestimates the firing rates of all three networks for moderate and strong drives; and the linear model with refractory, which has higher firing rates as explained earlier, underestimates the firing rates of the Sync model and overestimates that of the Hom model. Fig. 3C gives the percentage errors if the linear model with refractory was used to predict the firing rates of the network models. It confirms what is shown in Fig 3B (right).

For definiteness, we now focus on a single reduced model, namely the linear model with refractory, and refer to it simply as “the reduced model” in the rest of this section. There are likely many reasons why network firing rates are not in total

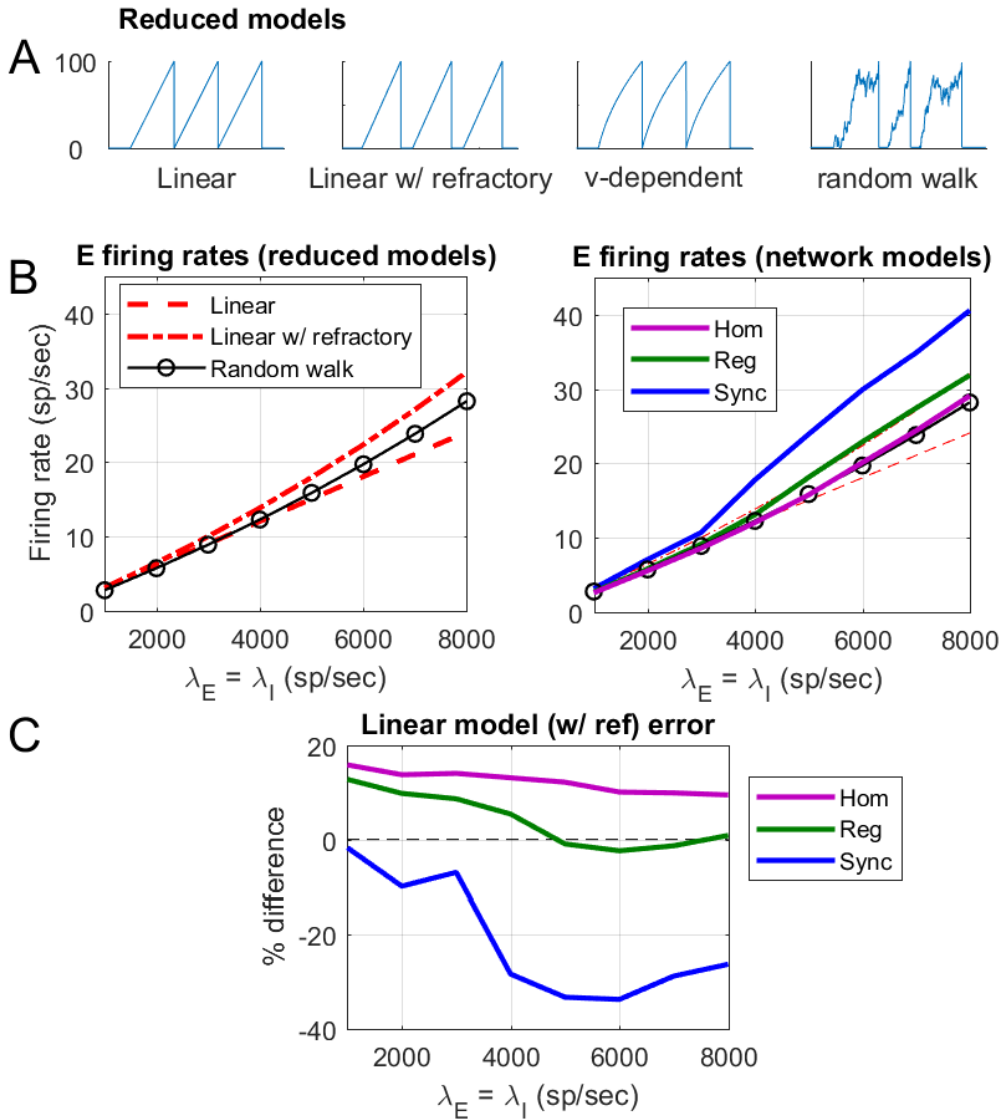


FIGURE 3. Comparison of firing rates. **A.** Trajectories of the membrane potential v as functions of time, for 4 reduced models. From left to right: the linear model, the linear model with refractory, the v -dependent model, and the random-walk model considered in Sect. 5. **B.** The left panel shows graphs of E-firing rates as functions of drive of the two linear reduced models, with and without refractory, and of the random walk model discussed in Section 5 (black with open circles). Firing rates of the v -dependent model are omitted as they cannot be computed reliably. The right panel shows firing rates of the network models (from Fig 1) superimposed on the graphs from the left panel. **C.** Percentage error if one uses the linear model with refractory to predict firing rates of network models. For example, -20% means the reduced model predicts a firing rate 20% lower than that of the network model.

agreement those of this reduced model. We will focus on two of them: correlated spiking in the form of partial synchronization as depicted in Figure 2, and the V -dependence of I-currents. The reason correlated spiking, or synchronization, may be relevant is that in this reduced model, the arrival of synaptic input to a neuron is assumed to be homogeneous in time. Indeed such an assumption is implicit (or explicit) in most reduced models, even though it is in direct contradiction to correlations in spiking or partial synchronization, phenomena that are well known to occur in the real brain.

One of the effects of correlated spiking is that a disproportionately large fraction of synaptic input may be missed during refractory. Some statistics pertinent to our investigation are shown in Fig 4. The bar graphs in Fig 4A show the percentages of E and I-spikes missed during refractory. Here we have distinguished between spikes from interactions among neurons within the population and from external drive. As external drive is assumed to be constant in time, one may equate the percentage of spikes from external drive missed with the percentage of time a neuron spends in refractory. As expected, the percentages of E- and I-spikes missed in the Hom network are reasonably close to those predicted by the reduced model. In the Sync network, the percentages of synaptic input missed are considerably higher than the percentage of time spent in refractory, consistent with the fact that spike times in this network are strongly correlated; see the correlation diagrams in Fig 2. That a smaller percentage of I-spikes are missed than E-spikes is likely due to τ^I being large relative to τ_R , so more I-spikes arrive after the neuron leaves refractory. Fig 4B shows the empirical mean values of V in the three network models, which are well above the mean values of V when I-spikes take effect.

Analysis. We now attempt to explain the deviations of network firing rates from those predicted by the linear model with refractory.

(a) *Discrepancy caused by lack of V -dependence of I-currents.* Our reduced model used S_{EI} and S_{II} values that correspond to network values at $V = M/2 = 50$. This choice is based on the assumption that V marches at constant speed from reset to threshold, and I-spikes arrive in a time-homogeneous way, neither of which is true and the situation is complicated: That I-spikes are stronger for larger V should cause mean V to be > 50 , but strong synchronization may cause more I-spikes to arrive when V is lower. Indeed according to Fig 4B, at drive=7000 sp/s, the mean V -value when I-spikes take effect are $\sim 54.5, 52$ and 48 respectively for the Hom, Reg and Sync networks. This means using S_{EI} and S_{II} values at $V = M/2$ underestimates the mean values of these parameters for the Hom and Reg networks, and overestimates it for the Sync network. Underestimating S_{EI} means that the network is in fact more suppressed than this reduced model suggests. To summarize: based on this one property alone, we would expect the reduced model to have a higher firing rate than the Hom and Reg networks (with a smaller error for the Reg network) and to have a lower firing rate than the Sync network.

(b) *The effects of partial synchronization working in concert with refractory.* Because the arrival of synaptic input is not necessarily homogeneous in time, the fraction

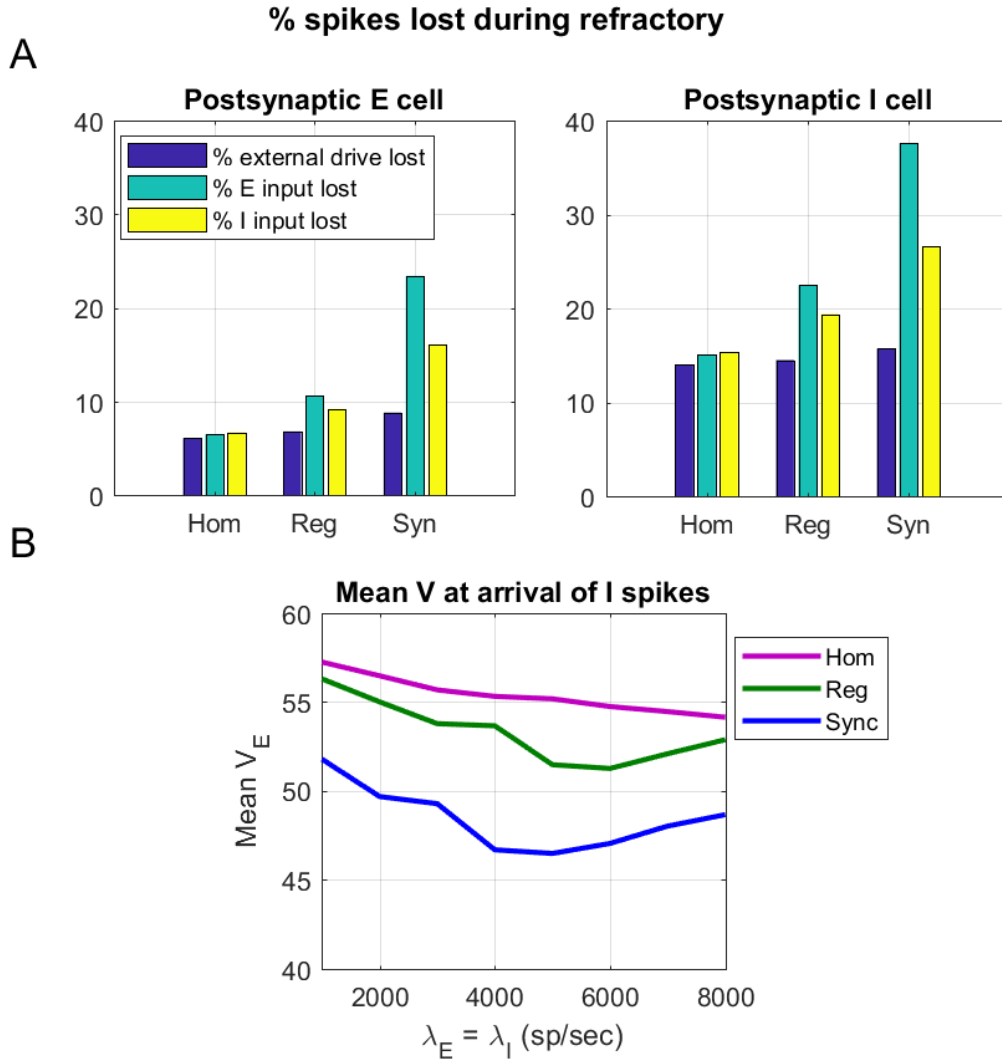


FIGURE 4. Challenging the homogeneity of drive assumption in reduced models. **A.** Percentages of external drive, E and I-spikes missed during refractory, for E and I neurons, for the Hom, Reg and Sync networks, for postsynaptic E-cells (left) and postsynaptic I-cells (right). The percentage of external drive missed can be taken to be % time spent in refractory; E and I input here refer to synaptic input from within the population. **B.** Mean V -values of E neurons (dashed) and mean V -values (solid) when I-spikes take effect, as functions of drive, for the three networks. Corresponding graphs for I-neurons are qualitatively similar.

of E and I-spikes “missed” during refractory can be nontrivially altered by partial synchronization. There is no easy way to predict the net effect of this phenomenon, however, because it involves both E- and I-inputs missed by both E and I neurons, leading to a not-so-simple cancellation problem.

Consider first E-neurons. Suppose an *additional* fraction ε_{EE} of E-input, and an additional fraction ε_{EI} of I-input, to E-neurons are lost during refractory – “additional” in the sense that it is above and beyond what is assumed to be lost during refractory under the homogeneity of input assumption. Then compared to the reduced model, there is a net gain in (positive) current in the amount of

$$\Delta F_E = \varepsilon_{EI} f_I C_{EI} - \varepsilon_{EE} f_E C_{EE} = 172 \varepsilon_{EI} f_I - 225 \varepsilon_{EE} f_E .$$

(This number can be positive or negative.) For an I-neuron, net gain relative to the reduced model is

$$\Delta F_I = \varepsilon_{II} f_I C_{II} - \varepsilon_{IE} f_E C_{IE} = 137 \varepsilon_{II} f_I - 300 \varepsilon_{IE} f_E .$$

For the Sync model, we see from Fig 4A that

$$\varepsilon_{EI} \approx 8, \quad \varepsilon_{EE} \approx 14.5, \quad \varepsilon_{II} \approx 11, \quad \varepsilon_{IE} \approx 22 .$$

With $\frac{3}{2}f_E < f_I < 3f_E$ (Fig 1), it is easy to see that ΔF_I is significantly more negative than ΔF_E . That is to say, synchronization causes I-neurons to lose more (positive) input current than E-neurons, so the system should be more excited and E-firing rate should be higher than predicted by the reduced model.

An analogous computation gives the same conclusion for the Reg network, but the difference between ΔF_E and ΔF_I is smaller. The $\varepsilon_{QQ'}$ values for the Hom network are too small to be significant.

Combining (a) and (b), we expect that the linear model with refractory will give E-firing rates that are higher than the Hom network (counting only the error from (a)), and lower than the Sync network (errors from both (a) and (b)). As for the Reg network, the two errors from (a) and (b) have opposite signs; one cannot say what it will be on balance except that it is likely to be smaller than the other two. This is consistent with the results in Fig 3B (right).

A general remark. We have found that ΔF_I is generally larger in magnitude than ΔF_E when input currents are changed, due simply to the fact that I-neurons have higher firing rates, we believe. These changes depend on the composition of the current that is altered, however, and in the situation above that depends on the relative speeds at which E and I spikes take effect, i.e., on τ^E and τ^I . A complete analysis of that is beyond the scope of this paper. We believe a separate mathematical model about the interaction of E and I spikes during a spiking event is necessary to address this issue. Thus while we have often seen that synchronization leads to higher firing rates, we do not know if this is always the case, or the conditions under which this is true.

5. MODELING MEMBRANE POTENTIALS AS RANDOM WALKS

In this section, we consider a different kind of reduced model, namely one in which membrane potentials of E and I neurons are modeled as (biased) random walks with reset at threshold. This model is in part motivated by the fact that reduced models defined by ODEs cannot reproduce the statistics of events observed in populations of interacting neurons, and that stochastic fluctuations – or population activity that give rise to behaviors that resemble stochastic fluctuations – seem to play a role in neuronal dynamics.

5.1. A random walk model and its firing rate. Here we model the membrane potentials of an E and an I-neuron by a continuous time Markov jump process (X_t^E, X_t^I) where X_t^E and X_t^I are independent and each takes values in the state space $\{-M_r, \dots, M-1, \mathcal{R}\}$. For definiteness we will consider a model that incorporates both refractory periods and the V -dependence of I-currents.

Given a pair (f_E, f_I) which represents the firing rates of excitatory and inhibitory neurons from the local population, we assume that X_t^E is driven by three independent Poisson processes that correspond to (i) external drive, (ii) excitatory and (iii) inhibitory synaptic inputs from the population. The Poisson process corresponding to (i) delivers kicks at rate λ^E . The ones corresponding to (ii) and (iii) have rate $N_E P_{EE} f_E$ and $N_I P_{EI} f_I$ respectively. Upon receiving a kick from the external drive, X_t^E moves up by 1. Upon receiving a kick from (ii), X_t^E jumps up by S_{EE} slots, and upon receiving a kick from (iii), it jumps down by $S_{EI}(X_t^E)$ slots. The interpretation of non-integer numbers of slots and the X_t^E -dependence of S_{EI} are as in Sect. 1.1. Also as before, when X_t^E reaches M , it goes to \mathcal{R} , where it remains for an exponential time of mean $\tau_{\mathcal{R}}$. The process X_t^I is defined analogously.

It is well known that an irreducible Markov jump process on a finite state space admits a unique stationary distribution. Given (f_E, f_I) , let ν_Q denote the stationary distribution of X_t^Q for $Q = E, I$. Clearly, ν_Q is a computable distribution satisfying

$$(5.1) \quad \begin{cases} \mathbf{A}_Q \nu_Q = \mathbf{0} \\ \mathbf{1}^T \nu_Q = 1 \end{cases}$$

where \mathbf{A}_Q is the generator matrix of process X_t^Q , and $\mathbf{1}$ is a vector in \mathbb{R}^{M+M_r+1} all of whose entries are equal to 1. The *firing rate* of X_t^Q , $Q \in \{E, I\}$, can be defined as

$$\tilde{f}_Q = \lim_{T \rightarrow \infty} \frac{1}{T} \#\{t \in (0, T) \mid X_{t-}^Q \neq \mathcal{R}, X_t^Q = \mathcal{R}\}.$$

It is easy to see that

$$\tilde{f}_Q = N_E P_{QE} f_E \sum_{i=M-S_{QE}}^{M-1} \nu_Q(i) + \lambda^Q \nu_Q(M-1).$$

Of interest to us is (f_E, f_I) satisfying the consistency condition $(f_E, f_I) = (\tilde{f}_E, \tilde{f}_I)$. We prove the existence of a solution to this consistency equation.

Theorem 5.1. *There exist $f_E, f_I > 0$ such that when (X_t^E, X_t^I) is driven by these firing rates, they produce mean firing rates \tilde{f}_E and \tilde{f}_I such that*

$$\tilde{f}_E = f_E, \quad \tilde{f}_I = f_I.$$

Proof. Let

$$\phi_1(f_E, f_I) = \tilde{f}_E - f_E \quad \text{and} \quad \phi_2(f_E, f_I) = \tilde{f}_I - f_I.$$

Observe that for any $f_I \geq 0$,

$$\phi_1(0, f_I) > 0 \quad \text{and} \quad \phi_1(f_E, f_I) < 0 \quad \text{when} \quad f_E > \tau_{\mathcal{R}}^{-1}.$$

The first inequality is true because independently of how high a rate the inhibitory clock rings, there exists $T_0 > 0$ and $\varepsilon > 0$ (depending on f_I) such that starting from anywhere in Γ , external drive alone will, with probability $\geq \varepsilon$, cause X_t^E to spike within T_0 units of time, rendering $\tilde{f}_E > 0$. The second inequality is true because each time X_t^E spikes, it has to spend time in refractory, so $\tilde{f}_E \leq \tau_{\mathcal{R}}^{-1}$. Similarly, observe that for any $f_E \geq 0$,

$$\phi_2(f_E, 0) > 0 \quad \text{and} \quad \phi_2(f_E, f_I) < 0 \quad \text{when} \quad f_I > \tau_{\mathcal{R}}^{-1}.$$

By the Poincare-Miranda Theorem (a version of intermediate value theorem in dimensions greater than one), we have the existence of a solution

$$\phi_1(f_E, f_I) = 0, \quad \phi_2(f_E, f_I) = 0.$$

Moreover, from the boundary conditions above, we have that $f_E, f_I > 0$. \square

Let f_E^{rw} and f_I^{rw} denote the mean firing rates obtained from Theorem 5.1. They were found to be unique in our numerical simulations, and very close to the empirical firing rates of the Hom network. See Fig 3B, the graph in black with open circles. That this graph is close to the one for the Hom network and somewhat below those of the Reg and Sync network models is consistent with our analysis in Sect. 4.2: Here we have corrected the error due to V -dependence but not the one due to the combined action of synchronization and refractory. As explained in Sect. 4.2, such action causes E-firing rates of the Sync and Reg networks to be higher than that predicted under the assumption that the arrival of synaptic input is homogeneous in time.

Sample paths of X_t^E in background ($\lambda^E = \lambda^I = 1000$) and when strongly driven ($\lambda^E = \lambda^I = 7000$) are shown in Fig 5A,B (top). We have included for comparison voltage traces of an E-neuron from the Reg model at corresponding drives directly below. These traces are very similar and not easily discernible by eye.

5.2. Interspike intervals. As noted earlier, the random walk (rw) model above has the capability of producing statistics that may emulate those in network models, something the reduced ODE models studied earlier cannot do. In this subsection, we focus on the distribution of interspike times, i.e., the times between consecutive spikes fired by a neuron. Histograms of interspike times from the rw model and the Reg network model are shown in Fig 5C. While not identical, they bear a clear resemblance.

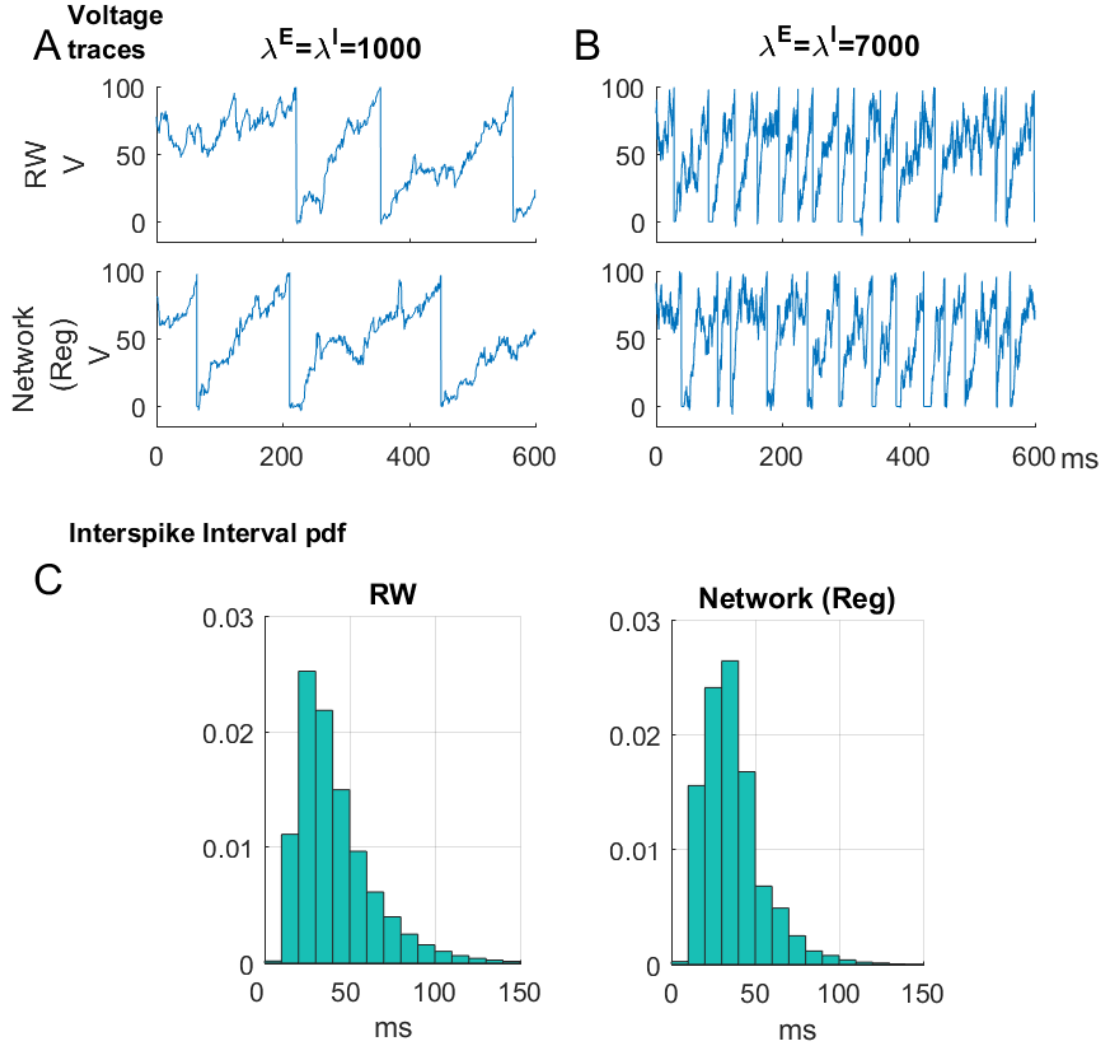


FIGURE 5. Trajectory of single neuron in network model vs. random walk. A-B. Sample paths of X_t^E are shown above traces of membrane potential of a randomly chosen neuron in the Reg network. A: background. B: strongly driven. C. Empirical distributions of interspike intervals for X_t^E (left) and for a neuron from the Reg network. In the definition of X_t^E , the same parameters as in the network models are used in the Poisson processes, and the firing rates used are (f_E^{rw}, f_I^{rw}) from Theorem 5.1.

Below we propose an explicit distribution that will be shown numerically to approximate well the distribution of interspike times for the rw model. We will then apply these ideas to the network models, and see how they fare.

Approximation of first passage times of the rw model by inverse Gaussians. For convenience, we consider a rescaling of (X_t^E, X_t^I) in which the interval $[0, M]$ is scaled linearly to $[0, 1]$, with jump sizes scaled accordingly. (We may assume for purposes of this discussion that jump sizes are given by $S_{QQ'}/M$ whether or not $S_{QQ'}$ is an integer.) Let us call this rescaled rw model (Y_t^E, Y_t^I) , and assume throughout that the population firing rates (f_E, f_I) are those obtained from Theorem 5.1. Let us also agree to ignore the time spent in refractory, which is entirely irrelevant in this discussion.

The random variables of interest, then, are T_E^{rw} and T_I^{rw} , the first passage times of Y_t^E and Y_t^I to 1 starting from $Y_0^E, Y_0^I = 0$. For definiteness, we will work with Y_t^E ; the analysis of Y_t^I is entirely analogous. Below we make a sequence of approximations that will result in an explicit distribution to be compared to that of T_E^{rw} .

(i) For a small time interval dt , we have

$$Y_{t+dt}^E \approx Y_t^E + G^E(Y_t^E, dt),$$

where

$$G^E(Y_t, dt) = \frac{S_{EE}}{M} \text{Pois}(N_E f_E P_{EE} dt) - \frac{S_{EI}}{M} (MY_t^E) \text{Pois}(N_I f_I P_{EI} dt) + \frac{1}{M} \text{Pois}(\lambda^E dt),$$

where $\text{Pois}(\lambda)$ is a Poisson random variable with parameter λ . All Poisson random variables are assumed to be independent. It is easy to see that

$$\mathbb{E}[G^E(Y_t^E, dt)] = \frac{1}{M} (S_{EE} N_E f_E P_{EE} - S_{EI} (MY_t^E) N_I f_I P_{EI} + \lambda^E) dt := b_E(Y_t^E) dt$$

and

$$\begin{aligned} \text{Var}[G^E(Y_t^E, dt)] &= \frac{1}{M^2} (S_{EE}^2 N_E f_E P_{EE} + S_{EI} (MY_t^E)^2 N_I f_I P_{EI} + \lambda^E) dt \\ &:= \sigma_E^2(Y_t^E) dt. \end{aligned}$$

(ii) Next we approximate $G^E(Y_t^E, dt)$ by a random variable $\hat{G}^E(dt)$ that is independent of Y_t^E . Specifically we seek $\hat{G}^E(dt)$ with the property that

$$\mathbb{E}[\hat{G}^E(dt)] = f_E dt \quad \text{and} \quad \text{Var}[\hat{G}^E(dt)] \approx \text{Var}[G^E(1/2, dt)] := \hat{\sigma}_E^2 dt,$$

i.e.,

$$\hat{\sigma}_E = \frac{1}{M} \sqrt{S_{EE}^2 N_E f_E P_{EE} + S_{EI} (M/2)^2 N_I f_I P_{EI} + \lambda^E}.$$

We leave it to the reader to check that the following might be a candidate:

$$\begin{aligned} \hat{G}^E(dt) &= \left(\frac{S_{EE}}{M} + \epsilon\right) \text{Pois}(N_E f_E P_{EE} dt) - \left(\frac{S_{EI}(M/2)}{M} - \epsilon\right) \text{Pois}(N_I f_I P_{EI} dt) \\ &\quad + \left(\frac{1}{M} + \epsilon\right) \text{Pois}(\lambda^E dt) \end{aligned}$$

where

$$\epsilon = \frac{f_E - b_E(1/2)}{M(N_E f_E P_{EE} + N_I f_I P_{EI} + \lambda^E)} .$$

(iii) It is well known that a Poisson distribution $\text{Pois}(\lambda)$ is approximated by $N(\lambda, \lambda)$ where $N(\cdot, \cdot)$ is the normal distribution when λ is large (usually larger than 10). In our model, the three constants $N_E f_E P_{EE}$, $N_I f_I P_{EI}$, and λ^E are $> 10^3$ for strong drive. Under these conditions, for $dt > 0.01$, the three Poisson distributions can be approximated by normal distributions. Since a linear combination of independent normal random variables gives a normal random variable, we have the approximation

$$Y_{t+dt}^E \approx Y_t^E + f_E dt + \hat{\sigma}_E dW_{dt} ,$$

where $dW_{dt} \sim N(0, dt)$.

(iv) The formula above is the Euler-Maruyama scheme for the stochastic differential equation

$$(5.2) \quad dZ_t = f_E dt + \hat{\sigma}_E dW_t \quad , \quad Z_0 = 0 .$$

This scheme is known to be strongly convergent, i.e., trajectories produced by the numerical scheme converges to trajectories of (5.2) when the step size approaches to 0 [16].

(v) Finally, for a (true) Brownian motion with a drift, given by

$$f_E t + \hat{\sigma}_E W_t ,$$

the first passage time to 1 starting from 0 is given by the inverse Gaussian $IG(f_E^{-1}, \hat{\sigma}_E^{-2})$ [10], where the inverse Gaussian $IG(\mu, \nu)$ is the probability distribution with density

$$\rho(x; \mu, \nu) = \left[\frac{\nu}{2\pi x^3} \right]^{\frac{1}{2}} \exp \left\{ \frac{-\nu(x - \mu)^2}{2\mu^2 x} \right\} .$$

We remark that we do not claim to have control over the cumulative errors in steps (ii), (iii) and (iv), and that the argument above is intended only to be heuristic. Numerically, it appears to be a good approximation, as can be seen in Fig 6A, where we have plotted the first passage times for Y_t^E and Y_t^I and their inverse Gaussian approximations.

Interspike times in network models and inverse Gaussians. The idea here is to start from a network model, pass to its accompanying rw model, find the appropriate IG distribution as discussed above, and use that to approximate the interspike times of the network model. The excellent match between inverse Gaussians and the pdf of interspike times for the Hom model can be seen in Fig 6B, both in background and under drive. The performance of this recipe is likely to deteriorate with increased synchronization: not only will synchronization change firing rate (hence the drift term in the approximation above) as discussed in Sect. 4.2, in the case of strongly synched networks the semi-regularity of spiking events will likely appear as semi-regularly spaced bumps in interspike time distributions. Still, in lower resolution the inverse Gaussian appears to be a decent approximation for the Reg network, as can be seen in Fig 6C.

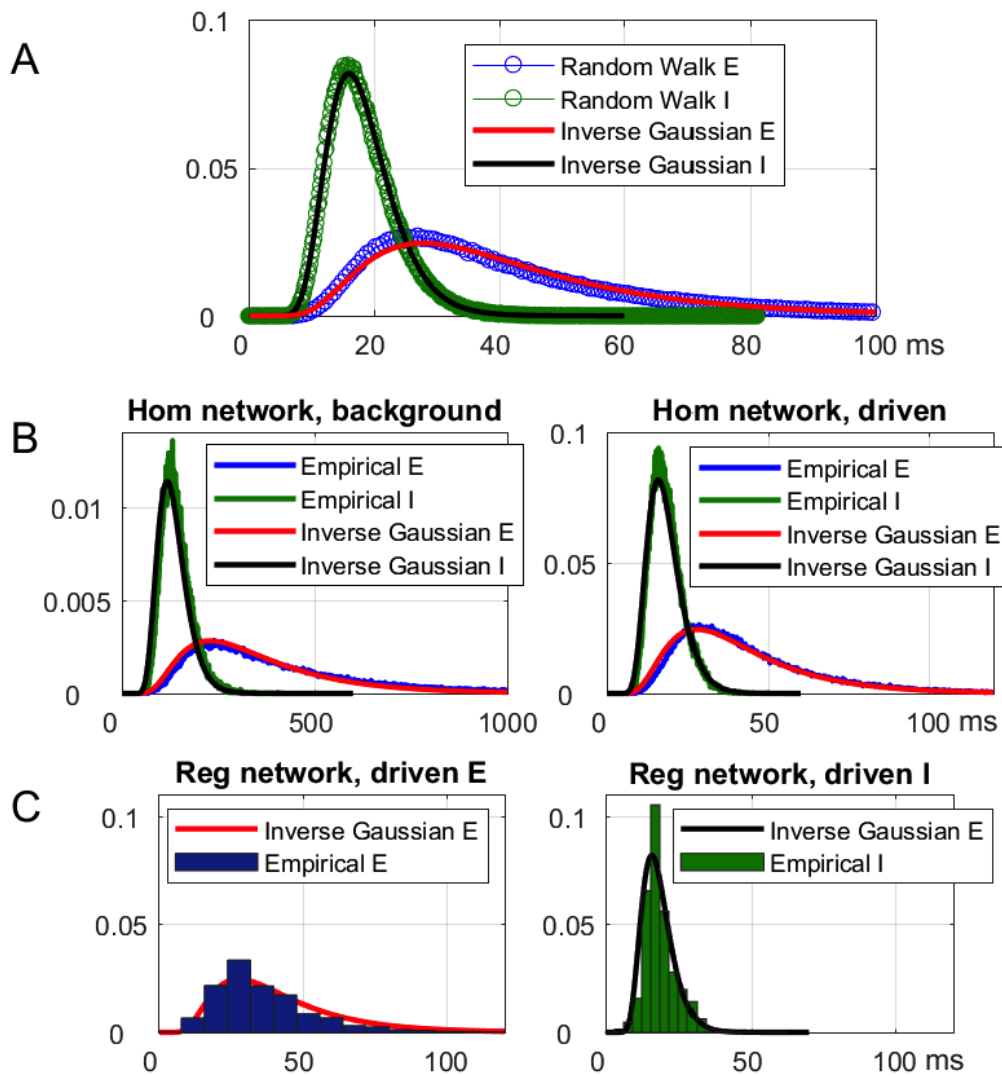


FIGURE 6. **Inverse Gaussians as approximations for distributions of interspike times.** A. Pdf of the inverse Gaussian distributions (solid lines, red for E, black for I) and empirical first passage time for Y_t^E and Y_t^I (open circles, blue for E, green for I). For parameters of the IG-distributions, see the main text. B. Comparison of inverse Gaussian distribution (red/black) and empirical interspike times from the Hom network (blue/green). Left: background. Right: strong drive. Resolution: 1000 bins. C. Comparison of inverse Gaussian distribution (red/black) and empirical interspike times from the Reg network (blue/green) at much lower resolutions. Left: E-interspike times. Right: I-interspike times. bins.

6. SUMMARY AND CONCLUSION

We introduced in Section 1 a family of stochastic networks of interacting neurons that we believe will be of independent interest, but for our purposes here, what is relevant is that these models have easily characterizable firing rates and correlation properties, which emerge as a result of the dynamical interaction among neurons.

We compared the firing rates of these network models to some very simple reduced models defined by a pair of ODEs representing the membrane potentials of an E and an I-neuron, taking care to give these neurons the mean excitatory and inhibitory currents received per unit time by E and I-neurons in the stochastic network models.

A property common to many reduced models including ours is the underlying assumption that all inputs received by a neuron arrive in a time-homogeneous way. This assumption contradicts directly the presence of correlations in neuronal spiking, which are observed in network models as in the real brain. It is arguably the single biggest difference between reduced and network models.

How exactly does the uneven arrival of input affect firing rate? Does the Ergodic Theorem not tell us that in the long run, the integral of the net current, roughly speaking, determines firing rate? The answer would have been yes had it not been for the “nonlinearities” present in the time evolution of membrane potentials. We have focused on two of these nonlinearities: refractory and the V -dependence of I-currents, and our findings can be summarized as follows:

A neuron “misses” a fraction of the spikes that it receives during refractory. The fraction missed is proportional to firing rate, so for a start refractory affects E and I neurons differently. The amount of current missed can be significant, and is exaggerated by synchronization. Furthermore, the composition of the missed current matters, and that has to do with relative spike times and conductance properties of E and I neurons. Synchronization also changes of the membrane potential of the postsynaptic neuron when I-spikes arrive, altering the strength of the suppression.

We demonstrated clearly how these nonlinearities affected firing rates in three example networks, using simulations to confirm the reasoning above. In these and other examples we have studied, the effects can be considered modulatory except when the network is highly synchronized, and the errors caused by the two nonlinearities above can add or cancel. We believe these pictures are quite typical, but obviously cannot draw more general conclusions.

In addition to the use of simple ODE models to predict firing rates, we have found that simple random walk models (again using currents from the network model to determine step sizes and biases) reproduce well fluctuations in membrane potentials and inter-spike time distributions of individual neurons in network models.

REFERENCES

- [1] Daniel J Amit and Nicolas Brunel, *Dynamics of a recurrent network of spiking neurons before and following learning*, *Network: Computation in Neural Systems* **8** (1997), no. 4, 373–404.
- [2] ———, *Model of global spontaneous activity and local structured activity during delay periods in the cerebral cortex.*, *Cerebral cortex* (New York, NY: 1991) **7** (1997), no. 3, 237–252.

- [3] Christoph Börgers and Nancy Kopell, *Synchronization in networks of excitatory and inhibitory neurons with sparse, random connectivity*, Neural computation **15** (2003), no. 3, 509–538.
- [4] Nicolas Brunel, *Dynamics of sparsely connected networks of excitatory and inhibitory spiking neurons*, Journal of computational neuroscience **8** (2000), no. 3, 183–208.
- [5] David Cai, Louis Tao, Aaditya V Rangan, David W McLaughlin, et al., *Kinetic theory for neuronal network dynamics*, Communications in Mathematical Sciences **4** (2006), no. 1, 97–127.
- [6] David Cai, Louis Tao, Michael Shelley, and David W McLaughlin, *An effective kinetic representation of fluctuation-driven neuronal networks with application to simple and complex cells in visual cortex*, Proceedings of the National Academy of Sciences of the United States of America **101** (2004), no. 20, 7757–7762.
- [7] Logan Chariker, Robert Shapley, and Lai-Sang Young, *Orientation selectivity from very sparse lgn inputs in a comprehensive model of macaque v1 cortex*, Journal of Neuroscience **36** (2016), no. 49, 12368–12384.
- [8] ———, *Rhythm and synchrony in recurrent cortical models*, Preprint (2017).
- [9] Logan Chariker and Lai-Sang Young, *Emergent spike patterns in neuronal populations*, Journal of computational neuroscience **38** (2015), no. 1, 203–220.
- [10] Raj Chhikara, *The inverse gaussian distribution: Theory: Methodology, and applications*, vol. 95, CRC Press, 1988.
- [11] Wulfram Gerstner, *Population dynamics of spiking neurons: fast transients, asynchronous states, and locking*, Neural computation **12** (2000), no. 1, 43–89.
- [12] Agnieszka Grabska-Barwińska and Peter E Latham, *How well do mean field theories of spiking quadratic-integrate-and-fire networks work in realistic parameter regimes?*, Journal of computational neuroscience **36** (2014), no. 3, 469–481.
- [13] Martin Hairer and Jonathan C Mattingly, *Yet another look at harris ergodic theorem for markov chains*, Seminar on Stochastic Analysis, Random Fields and Applications VI, Springer, 2011, pp. 109–117.
- [14] Evan Haskell, Duane Q Nykamp, and Daniel Tranchina, *A population density method for large-scale modeling of neuronal networks with realistic synaptic kinetics*, Neurocomputing **38** (2001), 627–632.
- [15] J Andrew Henrie and Robert Shapley, *Lfp power spectra in v1 cortex: the graded effect of stimulus contrast*, Journal of neurophysiology **94** (2005), no. 1, 479–490.
- [16] Peter E Kloeden and Eckhard Platen, *Numerical solution of stochastic differential equations*, vol. 23, Springer Science & Business Media, 2013.
- [17] Bruce W Knight, Dimitri Manin, and Lawrence Sirovich, *Dynamical models of interacting neuron populations in visual cortex*, Robot Cybern **54** (1996), 4–8.
- [18] Sean P Meyn and Richard L Tweedie, *Markov chains and stochastic stability*, Cambridge University Press, 2009.
- [19] Ahmet Omurtag, Bruce W Knight, and Lawrence Sirovich, *Dynamics of neuronal populations: The equilibrium solution*, SIAM Journal on Applied Mathematics **60** (2000), no. 6, 2009–2028.
- [20] Aaditya V Rangan and David Cai, *Maximum-entropy closures for kinetic theories of neuronal network dynamics*, Physical review letters **96** (2006), no. 17, 178101.
- [21] Aaditya V Rangan and Lai-Sang Young, *Dynamics of spiking neurons: between homogeneity and synchrony*, Journal of Computational Neuroscience **34** (2013), no. 3, 433–460.
- [22] ———, *Emergent dynamics in a model of visual cortex*, Journal of Computational Neuroscience **35** (2013), no. 2, 155–167.
- [23] Carl van Vreeswijk and Haim Sompolinsky, *Chaotic balanced state in a model of cortical circuits*, Neural computation **10** (1998), no. 6, 1321–1371.
- [24] Hugh R Wilson and Jack D Cowan, *Excitatory and inhibitory interactions in localized populations of model neurons*, Biophysical journal **12** (1972), no. 1, 1–24.
- [25] ———, *A mathematical theory of the functional dynamics of cortical and thalamic nervous tissue*, Biological Cybernetics **13** (1973), no. 2, 55–80.

YAO LI: DEPARTMENT OF MATHEMATICS AND STATISTICS, UNIVERSITY OF MASSACHUSETTS
AMHERST, USA

E-mail address: yaoli@math.umass.edu

LOGAN CHARIKER: COURANT INSTITUTE OF MATHEMATICAL SCIENCES, NEW YORK UNI-
VERSITY, NEW YORK, NY 10012, USA

E-mail address: bortkiew@gmail.com

LAI-SANG YOUNG: COURANT INSTITUTE OF MATHEMATICAL SCIENCES, NEW YORK UNI-
VERSITY, NEW YORK, NY 10012, USA

E-mail address: lsy@cims.nyu.edu